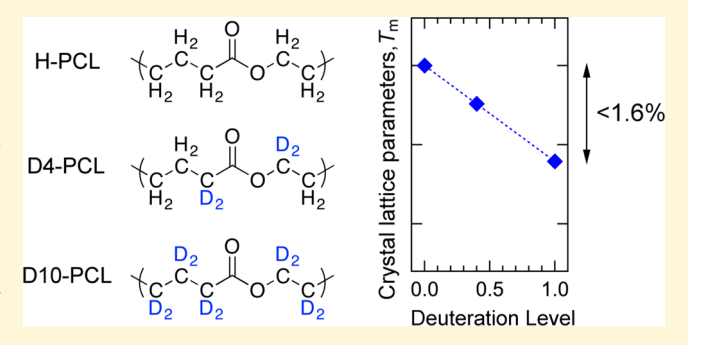
Selectively Deuterated Poly(ε -caprolactone)s: Synthesis and Isotope Effects on the Crystal Structures and Properties

Dongsook Chang,*,† Tianyu Li,†,‡ Lengwan Li,†,§ Jacek Jakowski,†,∥,⑥ Jingsong Huang,†,∥,⑥ Jong Kahk Keum,†,⊥ Byeongdu Lee,^{#,⑥} Peter V. Bonnesen,† Mi Zhou, ¶ Sophya Garashchuk,♠,⑥ Bobby G. Sumpter, , and Kunlun Hong*, , so

Supporting Information

ABSTRACT: Selective deuteration is an important tool for many analytical techniques including neutron scattering and spectroscopies. However, the availability of deuterated materials is limited because of the challenges in their synthesis. Here, we report the synthesis of partially and fully deuterated ε -caprolactone monomers and their corresponding polymers, poly(ε -caprolactone)s (PCLs), and the investigation of isotope effects on their crystalline structures and physical properties. Deuteration of PCLs leads to smaller crystal lattices and volumes compared to protiated PCLs by the amount proportional to the deuteration levels. The linear trend suggests that the volume isotope effect in PCL is



primarily governed by the vibrations of C-D and C-H bonds. The large intrachain contraction of deuterated PCLs compared to that of polyethylene reported in the literature can be ascribed to the presence of polar ester groups in PCLs. Deuterated PCLs also display lower melting temperatures than protiated PCLs proportional to their deuteration levels because of weaker intermolecular interactions in deuterated polymers. FTIR spectroscopy, with support from density functional theory calculations, shows large red shifts of the stretching and bending frequencies of C-D versus C-H bonds as dictated by their relative reduced masses $\sqrt{13/7}$, and to a smaller degree for the C=O stretching frequency. This work is among the very few studies comparing the effects of partial versus full deuteration on the structures and properties in semicrystalline polymers. These results not only advance our understanding of isotope effects in polymeric materials but also provide an important avenue to design polymers with desirable properties.

1. INTRODUCTION

Isotopic substitution of polymers or small molecular compounds has played an important role in many analytical techniques such as vibrational spectroscopy and nuclear magnetic resonance spectroscopy (NMR). Selective deuteration is one of the powerful tools for neutron scattering, highlighting (increasing scattering length density contrast) or dehighlighting (contrast matching) regions of interest because of the significant difference in scattering length densities for protium and deuterium. 1–3 Use of isotopic substitution including ²H, ¹³C, and ¹⁵N in solid-state NMR studies has

significantly contributed to the understanding of the structure and dynamics of polymer chains in semicrystalline polymers. 4-6 Deuteration is also useful to secondary ion mass spectrometry (SIMS) depth profiling,^{7,8} infrared spectroscopy peak assignment,9 and a recently developed technique based on broad-band coherent Raman microscopy¹⁰ that takes advantage of the mass difference between protium and

Received: August 28, 2018 Revised: October 26, 2018

Downloaded via UNIV OF SOUTH CAROLINA COLUMBIA on November 14, 2018 at 21:08:01 (UTC). See https://pubs.acs.org/sharingguidelines for options on how to legitimately share published articles.

[†]Center for Nanophase Materials Sciences, Oak Ridge National Laboratory, Oak Ridge, Tennessee 37831, United States

[‡]Department of Materials Science and Engineering and [§]Chemical & Biomolecular Engineering, University of Tennessee, Knoxville, Tennessee 37996, United States

Computational Sciences and Engineering Division, Oak Ridge National Laboratory, Oak Ridge, Tennessee 37831, United States ¹Chemical and Engineering Materials Division, Spallation Neutron Source, Oak Ridge National Laboratory, Oak Ridge, Tennessee 37831, United States

^{*}X-ray Science Division, Advanced Photon Source, Argonne National Laboratory, Argonne, Illinois 60439, United States

¹College of Materials Science and Engineering, Zhejiang University of Technology, Zhejiang 310014, China

Department of Chemistry and Biochemistry, University of South Carolina, 631 Sumter Street, Columbia, South Carolina 29208, United States

deuterium, enabling the elucidation of detailed molecular structures of polymer materials. It is clear that a diverse set of analytical tools are empowered by increasing availability of deuterated polymers and the development of deuteration chemistry.

At the same time, it is important to quantify and understand the seemingly trivial but non-negligible isotope effect in isotopically labeled materials. For example, there have been noteworthy physical properties affected by deuteration, including miscibility of deuterated polystyrene (dPS) with protiated polystyrene (PS) at high molecular weight, 11 optoelectronic properties of conducting polymers, 12,13 and crystallinity of conjugated polymers.

Effects of deuteration on molar volume and melting temperatures (T_m) have been reported in the literature, but these studies mainly concerned nonpolar polymers and provided limited information on the effects of deuteration level. 16-24 Molar volumes of fully deuterated polyolefins including polybutadienes, poly(vinylethylene), and polyethylene (PE) have been reported to be small based on crystal structure analysis 16 or density measurements. 23,24 $T_{\rm m}$ depression upon full deuteration has also been reported for *n*-hexatriacontane, ^{16–18} PE, ^{17,18} isotactic polystyrene (iPS), ¹⁹ and isotactic polypropylene (iPP), 20 as well as upon partial deuteration for PE and syndiotactic polypropylene (sPP). 21,22 Except for one study on partially deuterated PE suggesting a linear relationship between $T_{\rm m}$ depression and deuteration level,21 the effects of deuteration level have not been well documented. This knowledge gap at least partially originates from the difficulty in obtaining polymers with the degree of deuteration as a well-controlled variable.

From a quantum mechanical perspective, the change in properties imparted by deuteration is mainly related to the dynamic characteristics of C-H and C-D bonds. 15 A C-D bond has a lower harmonic vibrational frequency and zeropoint energy (ZPE) than a C-H bond because of the heavier mass of deuterium. The wave function of deuterium is slightly compressed compared to that of protium. Consequentially, the length of the C-D bond is shorter than that of the C-H bond by approximately 0.005 Å due to the lower ZPE and anharmonicity of the potential energy. ^{16,25} In addition to its shorter bond length, the C-D bond is less polarizable than the C–H bond, which leads to weaker intermolecular interactions of deuterated compounds. 14 The observed $T_{\rm m}$ depression of nonpolar polymers upon deuteration is primarily attributed to such weaker intermolecular interactions. ¹⁶ The volume isotope effects in deuterated polymers are explained by the smaller vibrational amplitude of the C-D bond and their shorter length, balanced by weaker intermolecular interactions.²⁶ However, it is less understood how deuteration affects those properties in polymers containing heteroatoms other than C and H/Ds.

Poly(ε -caprolactone) (PCL), an aliphatic polyester, has received much attention for various applications because of its characteristic properties. PCL can be enzymatically degraded by many microorganisms in nature. In addition to its favorable physical properties and broad compatibility with other polymers, the biodegradability of PCL has led to its use in environmentally friendly commercial products. PCL slowly degrades in physiological conditions by hydrolysis, and the fact that the degraded products are resorbable allow PCL to find a wide range of biomedical applications. The versatility of PCL combined with its simple chemical structure

has enabled it to become a model polymer in fundamental studies on various aspects of polymer crystallization. $^{31-34}$ Despite those intensive studies, the effects of deuteration on the molar volume and $T_{\rm m}$ in PCLs, and the implications of the presence of ester groups in these effects, have not been explored. PCL bears a resemblance to the well-studied PE structurally due to the aliphatic $-{\rm C_5H_{10}-vs}$ $-{\rm C_2H_4-chain}$ segments, and yet it is expected that the presence of the ester $-{\rm COO-functionality}$ in PCL plays a major role in affecting their structures and properties upon deuteration.

In this study, we present for the first time (i) the synthesis of selectively deuterated ε -caprolactone monomers and their corresponding polymers and (ii) the studies of deuteration effects on the crystal structures and physical properties of the PCL polymers. We focus on isotope effects on their unit cell volume and $T_{\rm m}$ depression as compared with similar effects on nonpolar polymers reported previously. Fourier-transform infrared spectroscopy (FTIR) is employed in conjunction with theoretical calculations to shed light on the effect of H/D isotopic substitution on structure dynamics in PCL and the role of the polar ester groups on the molecular interactions within the polymer chains. The precision synthesis of these monomers allows us to elucidate the effects of deuteration level and pinpoint the origin of the isotope effects.

2. EXPERIMENTAL SECTION

Materials. All reagents were used as received from the suppliers without further purification unless otherwise noted. Anhydrous toluene, CH₂Cl₂, chloroform, and methanol were purchased from Fisher Scientific. ε-Caprolactone (99%) and Sn(Oct)₂ (92.5–100.0%) were obtained from Sigma-Aldrich. 2-Methyl-1,3-propanediol (99%) was received from Oakwood Chemical. Cyclohexanone- d_{10} (Lot PR-27303B; nominally ~98 atom %D) was purchased from Cambridge Isotopes Laboratories, Inc. By ¹³C NMR analysis, the actual deuterium distribution was found to be ~94 atom %D at the α-carbon to the carbonyl (with a -CD₂- to -CDH- ratio of about 88:12) and ≥98 atom %D at the β- and γ-carbons.

Synthesis of Partially and Fully Deuterated Caprolactone **Monomers.** 2,2,6,6-Tetradeuterocyclohexanone. Cyclohexanone (20.0 g, 0.20 mol) was diluted with a mixture of tetrahydrofuran (THF, 30 mL) and dichloromethane (CH₂Cl₂ 10 mL) in a 200 mL round-bottom recovery flask. To this solution was added 25 g of 0.5 M potassium carbonate in deuterium oxide, and the rapidly stirred mixture was heated in a 68 °C oil bath for 21 h. The mixture separated into two phases upon cooling. A 50 µL aliquot from the upper organic phase was diluted with 700 μ L of CDCl₃ for proton and carbon NMR analysis, which revealed the cyclohexanone to be about 79 atom %D at the 2- and 6-positions. The phases were separated, and the aqueous phase was extracted with CH_2Cl_2 (2 × 25 mL). The CH₂Cl₂ extracts were combined with the organic phase and returned to the flask along with 10 mL of THF and 28 g of fresh 0.5 M potassium carbonate in deuterium oxide. About half of the CH₂Cl₂ was removed by rotary evaporation, and the remaining mixture was then heated as before. NMR analysis revealed the cyclohexanone to be about 87 atom %D. The workup and exchange procedure were repeated a third time (93 atom % D) and then a final time, affording 97 atom %D overall. The final organic solution was dried through a column of anhydrous granular sodium sulfate and diluted with additional CH2Cl2 to a total mass of 220 g (about 170 mL total volume). This solution was then used in the subsequent step.

2-Oxepanone-3,3,7,7- d_4 (ε -Caprolactone- d_4). The solution from above containing nominally 0.20 mol of 2,2,6,6-tetradeuterocyclohexanone in ca. 150 mL of dry CH₂Cl₂ was combined in a 2-L flask with Bi(III) triflate (6.56 g, 10.0 mmol) and diluted with additional dry CH₂Cl₂ (500 mL). The flask was cooled in an ice bath under nitrogen flow, and a suspension of *meta*-chloro-peroxybenzoic acid (m-CPBA, 72 g at 70–75% purity) in 150 mL dry CH₂Cl₂ was added.

The reaction was conducted in the same manner as described below for ε -caprolactone- d_{10} . The crude ε -caprolactone- d_4 was purified by fractional vacuum distillation from powdered calcium hydride (CaH₂). The yield on the high purity center cut distilling at 55–57 °C at ca. 0.5 mmHg was 17.1 g (72% overall yield from cyclohexanone) and had a chemical purity of \geq 99%. The monomer was stored frozen under nitrogen until ready to use.

2-Oxepanone-3,3,4,4,5,5,6,6,7,7- d_{10} (ε -Caprolactone- d_{10}). To a stirred suspension of dry CH₂Cl₂ (650 mL), Bi(III) triflate (6.56 g, 10.0 mmol), and cyclohexanone- d_{10} (21.65 g, 200 mmol), cooled in an ice bath under nitrogen flow, was added a suspension of metachloro-peroxybenzoic acid (m-CPBA, 73 g at 70-75% purity) in 150 mL dry CH₂Cl₂. The suspension was stirred an additional 30 min in the ice bath under nitrogen, whereupon the bath was removed and stirring continued for 4 h as the suspension warmed to laboratory temperature. The milky white suspension was then filtered (to remove insoluble Bismuth salts and some of the meta-chlorobenzoic acid that formed and precipitated), the solids were washed with CH₂Cl₂ (2 × 50 mL), and the combined CH₂Cl₂ filtrate and washings were returned to the 2 L reaction flask. A solution of saturated Na₂S₂O₃ (400 mL) was added with rigorous stirring, to convert any excess meta-chloro-peroxybenzoic acid still present to meta-chlorobenzoic acid. The aqueous phase became dark brown within 5 min, and stirring was continued at laboratory temperature for 1 h, during which additional white-gray solids are observed to form. The reaction is filtered, and the solids (mostly meta-chlorobenzoic acid) were washed with CH_2Cl_2 (2 × 100 mL). The mixed phase filtrate and washings were then transferred to a 2 L separatory funnel, and the lower CH2Cl2 phase was collected. The aqueous phase was then washed with CH_2Cl_2 (2 × 100 mL), to extract any ε -caprolactone that remained in the aqueous phase, and the washings were added to the main CH2Cl2 phase. This combined CH2Cl2 phase was then washed with 1 M Na₂CO₃ (4 × 250 mL) to extract out any remaining metachlorobenzoic acid. The aqueous Na2CO3 wash solutions were combined and then back-extracted with fresh CH₂Cl₂ (2 × 100 mL) to extract any ε -caprolactone present in this aqueous phase. The combined CH2Cl2 phases were then dried through a column of granular anhydrous Na₂SO₄, and the CH₂Cl₂ was removed by rotary evaporation at 35-40 °C to afford the crude ε -caprolactone- d_{10} in near-quantitative yield. Final purification was accomplished by fractional vacuum distillation from powdered calcium hydride (CaH₂). The yield on the high purity center cut distilling at 55-57 °C at ca. 0.5 mmHg was 20.77 g (84% yield) and had a chemical purity of ≥99%. The monomer was stored frozen under nitrogen until time of use.

Ring-Opening Polymerization. H-PCL, D4-PCL, and D10-PCL were synthesized by ring-opening polymerizations of ε -caprolactone, ε -caprolactone- d_4 , and ε -caprolactone- d_{10} , respectively, with a difunctional initiator (2-methyl-1,3-propanediol) and Sn(Oct)₂ as a catalyst.³⁵ A typical polymerization procedure was as follows: A 1 M Sn(Oct), solution in anhydrous toluene was prepared under an inert atmosphere. Then, 2-methyl-1,3-propanediol (13.4 mg, 0.15 mmol), the appropriate ε -caprolactone monomer (18.62 mmol), and 74.5 μ L of Sn(Oct), solution were added into a Schlenk flask with a magnetic stir bar. Evacuation-nitrogen refill processes were repeated three times, and the reaction was performed at 115 °C under a nitrogen atmosphere with vigorous stirring. H-PCL was polymerized overnight, while polymerizations of D4-PCL and D10-PCL were allowed to proceed for 72 h because of the slower polymerization kinetics of the deuterated monomers. The reaction mixtures were cooled to rt and precipitated three times in methanol from CH₂Cl₂.

Characterization. ¹H and ¹³C NMR spectra were obtained on a Varian VNMRS 500 NMR spectrometer at rt in CDCl₃ (7.27 ppm ¹H reference and 77.23 ppm ¹³C reference) unless otherwise noted. ¹³C NMR spectra were obtained using inverse-gated decoupling with a recycle delay of 25 s and reported for the deuterated monomers (Figure S1) as well as H-PCL, D4-PCL, and D10-PCL polymers (Figures S2-S4). The molar masses of the synthesized PCLs were determined with a size exclusion chromatography (SEC) system with an Agilent 1310B 1260 Infinity Isocratic HPLC pump equipped with

a multiangle static light scattering detector with a 664 nm laser (DAWN HELEOS-II, Wyatt) and a refractive index (RI) detector with a 658 nm laser (Optilab T-rEX, Wyatt). Four Phenomenex Phenogel columns in series (two 10^5 Å, one 10^4 Å, one 10^3 Å porosities, respectively; $10~\mu m$ particle size and 300 mm by 7.8 mm column dimensions, each) were used, and THF was the eluent with a flow rate of 1 mL/min. The dn/dc in THF values of polymers were measured to be 0.067, 0.061, and 0.052, for H-PCL, D4-PCL, and D10-PCL, respectively, in a separate batch mode (Figure S5). Absolute molar masses and dispersities were calculated from the collected RI and light scattering results using the measured dn/dc values.

For high-resolution powder X-ray diffraction (HRPD) measurements, polymer melts at 80 °C were allowed to fill Kapton capillaries (ID 0.76 mm, OD 0.864 mm) based on capillary motion under vacuum. The packed capillaries were cooled down to rt at approximately 0.2 °C/min. HRPD data were collected using beamline 11-BM at the Advanced Photon Source (APS), Argonne National Laboratory using an average wavelength of 0.412718 Å. Discrete detectors covering an angular range from -6° to 16° 2θ were scanned over a 34° 2θ range, with data points collected every 0.001° 2θ and scan speed of 0.01°/s. Small angle X-ray scattering (SAXS) was performed on the samples prepared for HRPD without further processing. Data were collected at 12-ID-B at APS with X-ray energy of 14 keV. The 2D data collected with Pilatus2M detector located at 3.6 m downstream of samples were converted to 1D using silver behenate as an angle standard. Exposure time was typically 0.1 s.

Differential scanning calorimetry (DSC) measurements were performed using TA Instruments (Q2000) under nitrogen flow. Approximately 4 mg of purified polymers were loaded to Hermatic aluminum pans. The samples were first heated to 80 $^{\circ}$ C at 10 $^{\circ}$ C/min and equilibrated for 10 min to erase thermal history. For ramp experiments, a subsequent cool/heat cycle was carried out at 2.5 °C/ min. The data presented in the main text were taken from the second heating/cooling curves. The sample preparation and DSC measurement were repeated three times to obtain average and standard deviations. For estimation of the equilibrium melting temperatures, polymers melted at 80 $^{\circ}\text{C}$ were isothermally crystallized at a desired temperature, and the melting temperature during subsequent heating at 10 °C/min was recorded. Polymers were allowed to crystallize for a predetermined time based on preliminary kinetics measurements to ensure their crystallinities did not exceed approximately 10% of the total crystallinity (based on the enthalpy of crystallization) to minimize crystal thickening.

FTIR was recorded in attenuated total reflection (ATR) geometry using a Bruker Optics Vertex 70 spectrometer equipped with a DTGS detector. PCL samples were prepared by first melting at 80 °C and cooling down to rt at approximately 0.2 °C/min in a vacuum oven. The solids were loaded to the diamond ATR crystal on a Harrick Scientific MVP 2 Series accessory, and 32 scans at 2 cm⁻¹ resolution were collected for samples. A background spectrum (32 scans at 2 cm⁻¹ resolution) of the clean ATR crystal was used as the reference. For a temperature-controlled experiment, a PIKE VeeMAX III accessory with a Ge crystal was used at an 80° incidence angle. Polymer powders were positioned on the crystal and backed by a silicon wafer. The temperature was controlled using Pike TempPRO software and ramped up to 70 °C at 10 °C/min and equilibrated for 10 min before cooling under ambient conditions. 96 scans at 4 cm resolution were collected each for the sample and the silicon wafer background. Baseline was corrected using a rubberband correction method using the built-in instrument software package (OPUS).

Theoretical Calculations. To develop a deep understanding of the effects of deuteration on the FTIR properties of PCL, we performed a series of vibrational normal-modes calculations. First, the crystal structure model of PCL was based on the coordinates of C and O atoms of PCL determined by X-ray diffraction (XRD).³⁶ H atoms were added on the aliphatic C atoms based on the expected sp³ hybridization. A structural optimization was performed for H atoms using density functional theory (DFT) with the Perdew–Burke–Ernzerhof (PBE) exchange-correlation functional,³⁷ with the Vienna

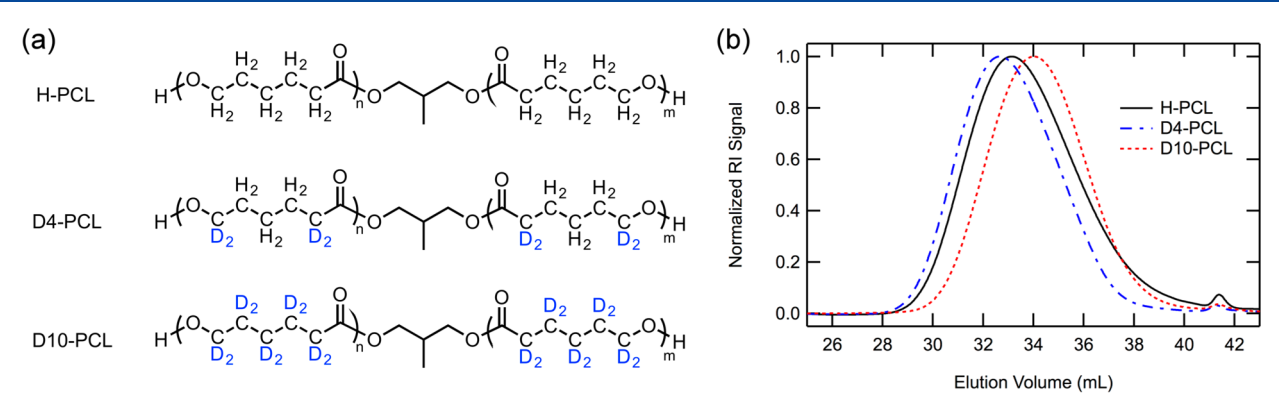
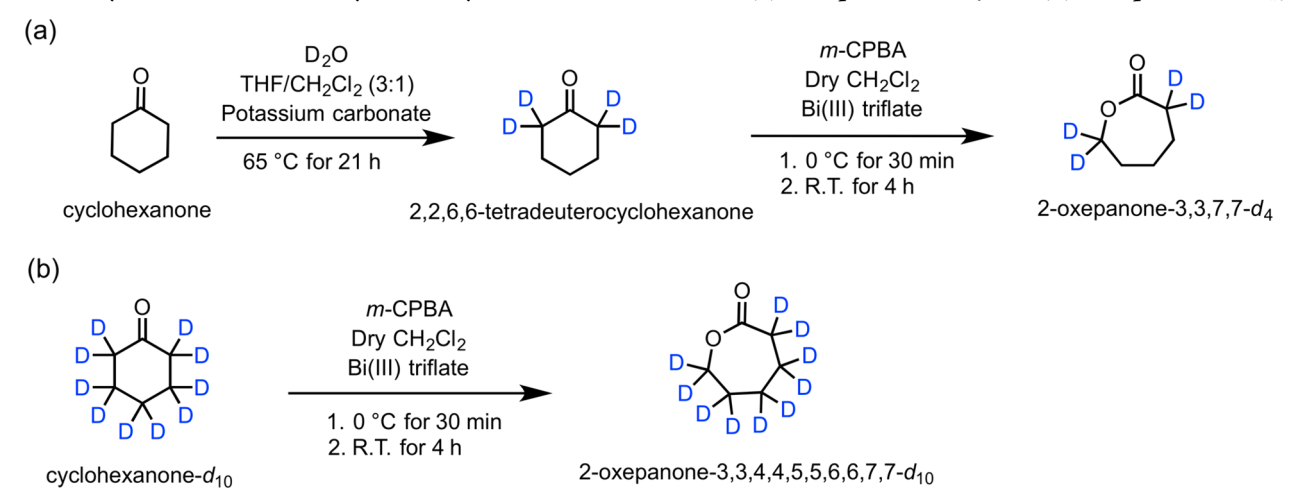


Figure 1. Selectively deuterated poly(ε -caprolactone)s used in the study. (a) Structures of PCLs with deuterated positions highlighted in blue and (b) their SEC traces obtained in THF.

Scheme 1. Synthesis of the Partially and Fully Deuterated Monomers: (a) ε -Caprolactone- d_4 and (b) ε -Caprolactone- d_{10}



Ab Initio Simulation Package (VASP).³⁸ The Kohn–Sham equations were solved using the projector-augmented wave (PAW) method, ^{39,40} along with standard PAW potentials for the constituent elements. The kinetic energy cutoff for the plane wave basis was set to 500 eV, the convergence criterion for electronic self-consistency was set to 10^{-5} eV, and the "accurate" precision setting was employed to avoid wraparound errors. The Brillouin-zone integration was performed on a Γ -centered 2 \times 2 \times 1 k-point grid. During the structural optimization, the lattice vectors were fixed while the atomic positions for the added H atoms were relaxed until the force criterion of 0.01 eV/Å was satisfied.

Vibrational frequency calculations were performed using a finite sized cluster model constructed from the crystal structural modelwith the QChem package.⁴¹ The cluster model consisted of one PCL chain at the center surrounded by 6 closely packed neighbors. Each PCL chain had 2 caprolactone units and was terminated with 2 H atoms to passivate the dangling bonds. Overall the 7-chain cluster had 266 atoms including 14 terminating H atoms. Partial optimization and vibrational analysis were performed for 18 atoms of a full caprolactone unit in the middle section of the central chain. Vibrational frequencies of the protiated and deuterated PCLs were used to simulate the IR spectra. Additional atoms on the same chain of the caprolactone unit and from neighboring chains were also included in the analyses to examine the isotope effects on the vibrational modes and frequencies. The calculations were performed at the DFT level, using the Long Range Corrected (LRC) hybrid density functional ωPBEh with Grimme's empirical dispersion correction (DFT-D), employing the 6-31G* basis set. 41 The ω PBEh functional was chosen, as it has been thoroughly tested and has shown good accuracy for a variety of ground and excited state properties.

3. RESULTS AND DISCUSSION

Synthesis of Deuterated Caprolactones and PCLs. To study the isotope effects from selective deuteration, we synthesized three PCLs with different deuteration levels, designated as H-PCL, D4-PCL, and D10-PCL, respectively, as shown in Figure 1a. H-PCL and D10-PCL are fully protiated and deuterated, respectively. D4-PCL is selectively deuterated at the two C atoms adjacent to the ester group. This allows us to probe the difference of deuteration effects at the C atom positions that are adjacent to or far from the ester group (see the FTIR section).

The synthesis of the ε -caprolactone- d_4 and ε -caprolactone- d_{10} monomers are illustrated in Scheme 1. To the best of our knowledge, neither ε -caprolactone- d_4 nor ε -caprolactone- d_{10} are commercially available. Although their preparations have appeared previously in the open literature, no detailed synthetic procedures amenable to large-scale synthesis have been reported. Tabet et al. have synthesized partially deuterated caprolactones by hydrogenation of deuterated olefinic lactones, but provided no synthetic details. Ottewill et al. briefly described the Baeyer-Villager oxidation to convert cyclohexanone- d_{10} to ε -caprolactone- d_{10} with m-CPBA in 21 h. However, the crude ε -caprolactone- d_{10} obtained was used directly in a subsequent reaction, and no yield or spectroscopic information for ε -caprolactone- d_{10} was presented. Accordingly, we have sought to develop efficient

synthetic procedures for these monomers with high deuteration levels at designated positions.

Through a collaboration via a CNMS User Project (see Acknowledgments), it was brought to our attention that bismuth triflate (Bi(OTf)₃) had been successfully employed to accelerate the well-known Baeyer-Villager oxidation of cyclohexanone to caprolactone. Specifically, Adapa and coworkers reported that use of 5 mol % bismuth triflate (Bi(OTf)₃) resulted in quantitative conversion of cyclohexanone to ε -caprolactone in 30 min. This reaction was reported at a 2 mmol scale, and we found it necessary to modify the procedure slightly when scaling up the reaction 50to 100-fold. These modifications included extending the reaction time and reducing the amount of m-CPBA (70-75% activity) used from 200 mol % to ~150 mol %. These conditions worked quite well for ca. 20-g scale reactions, with essentially no H/D back-exchange observed during the purification procedures. The deuteration levels of the purified ε -caprolactone- d_4 and ε -caprolactone- d_{10} monomers were found to be 97% and 98% by ¹³C NMR, respectively (Figure S1).

PCLs were synthesized from the obtained caprolactones through ring-opening polymerization, adapted from a previously published method.³⁵ We have chosen a difunctional initiator, 2-methyl-1,3-propanediol, to avoid a potential endgroup effect in future studies. We have aimed to match the number of repeat units per chain considering that crystallinity as well as crystallization and melting kinetics of PCL depend on the degree of polymerization,^{33,46} and polymer samples with approximately 10 kg/mol molar masses are selected for this study. SEC of the PCLs shows their hydrodynamic sizes in THF closely match one another (Figure 1b). Molar mass, dispersity, and degrees of polymerization of these polymers are summarized in Table 1.

Table 1. Characteristics of PCLs Used in This Study

polymers	$M_{\rm n}$ (g/mol)	dispersity	DP^a			
H-PCL	11 000	1.25	96			
D4-PCL	13 000	1.26	110			
D10-PCL	11 100	1.21	89			
^a Degree of polymerization (DP) = $n + m$ in Figure 1a.						

Crystal Lattice Parameters and Molar Volumes. Following the successful synthesis, next we examined the changes of structural parameters caused by deuteration. HRPD curves of these polymers crystallized at the same cooling rate from melt were obtained using a synchrotron powder

diffractometer (Figure 2a). Diffraction peaks of H-PCL are indexed based on the reported *d*-spacings of PCL crystal in the literature. 47 The lattice parameters are determined to be a =7.502 Å, b = 4.972 Å, and c = 17.254 Å (fiber axis) from the three most pronounced peaks, (200), (110), and (111) of H-PCL. Good agreement of the lattice parameters with literatures 36,47,48 suggests that the presence of the difunctional initiator in the middle of the PCL chains and the consequent inversion of ester group direction within a chain have no noticeable impact on their crystal structures, which is reasonable considering chain folding that usually occurs in crystallization. 49-51 Structural peaks of D4-PCL and D10-PCL appear slightly shifted to higher diffraction angles (Figure 2b), suggesting their smaller crystal lattices compared to H-PCL. Lattice parameters and molar volume ratios are calculated for H-PCL, D4-PCL, and D10-PCL and summarized in Table 2 along with their percentage reductions.

The linear dependence of crystal lattice parameters and molar volume on deuteration level is demonstrated in Figure 3. The lattice parameters changes of deuterated PCLs compared to those of H-PCL reveal that the degree of reduction is linearly proportional to deuteration level in all three lattice directions, with the largest reduction along the c-axis (Figure 3a). As a result, the ratios of the molar volume of protiated species to that of deuterated species (V_H/V_D) also show a linear relationship with deuteration level; that is, 40% deuteration of the aliphatic chain in D4-PCL leads to precisely 40% reduction of molar volume compared to that of D10-PCL (Figure 3b). The origin of molar volume reduction in hydrocarbons is explained in the literature mainly by the larger vibrational amplitude of the C-H bond in addition to effects from bond length and polarizability.²⁶ Similarly, the linear relationship in our results indicates that the volume isotope effect in PCL is primarily determined by deuteration level, and is related less to the specific deuteration sites for D4-PCL. To the best of our knowledge, this work is the first to show the relationship between crystal lattice parameters and the deuteration level of polymers. We expect that preparation of PCLs with other deuteration levels in the future will help corroborate the finding.

The significant c-axis reduction in PCL is particularly noteworthy when compared with the lattice parameter changes of PE (Table 2). PE and PCL have similar orthorhombic crystal structures with their chains arranged parallel to the c-axis in zigzag conformation. The a, b lattice parameters of PCL are slightly larger than those of PE due to the presence of carbonyl groups in PCL that are perpendicular to the polymer chain. 47,53 Both polymers display similar degrees of volume

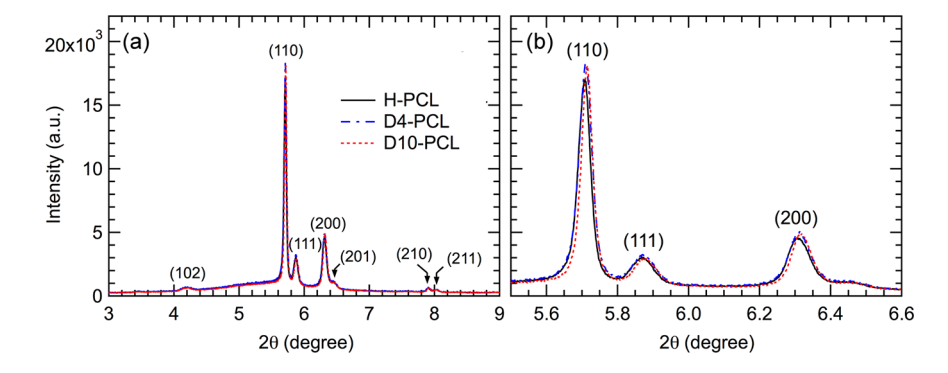


Figure 2. HRPD results showing (a) overall diffraction curves and (b) expanded view of the (110), (111), and (200) peaks.

Table 2. Lattice Parameters and Molar Volume Ratios Calculated for Selectively Deuterated PCLs Compared with That of Protiated and Deuterated PEs (H-PE and D-PE, respectively) from Literature

polymers	$a (Å)^a$	b (Å) ^a	c (Å) ^a	$V_{ m H}/V_{ m D}^{}$	reference
H-PCL	7.502	4.972	17.254	1.0000	this work
D4-PCL	7.497 (-0.065%)	4.971 (-0.032%)	17.229 (-0.145%)	1.0024	this work
D10-PCL	7.491 (-0.149%)	4.968 (-0.093%)	17.191 (-0.365%)	1.0061	this work
H-PE	7.42	4.87	2.546	1.0000	52
D-PE	7.41 (-0.33%)	4.85 (-0.19%)	2.546 (0%)	1.0052	16

^aPercentage reductions are shown by numbers in parentheses. ^bRatio of molar volume of protiated polymer to molar volume of (partially or fully) deuterated polymer, following the convention in literature. ¹⁶

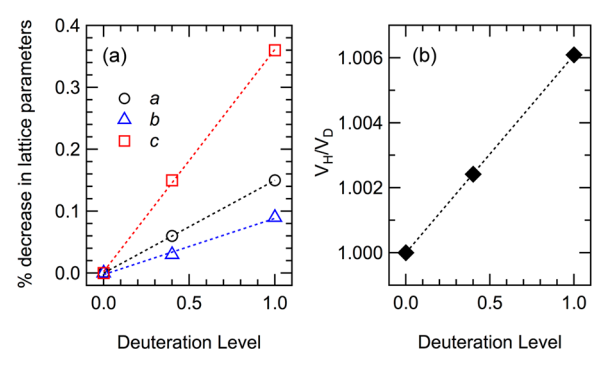


Figure 3. Structural parameters extracted from HRPD measurements as a function of deuteration level. (a) Percentage reduction of crystal lattice parameters, and (b) the ratio of molar volumes $(V_{\rm H}/V_{\rm D})$ as a function of deuteration level. Linear fits are shown as dotted lines in both plots.

isotope effects upon full deuteration as represented by their comparable $V_{\rm H}/V_{\rm D}$ ratios. Despite these similarities, only a, b lattice parameters of PE decrease by deuteration with no change in the c parameter observed within experimental resolution, 16 while PCL shows the largest reduction in the c-axis. In other words, volume isotope effects in PE are manifested by reduction in their interchain distances, while that in PCL occurs through significant intrachain contraction in addition to the small reduction in the interchain distances.

The larger c-axis reduction upon deuteration of PCL compared to that of PE can be attributed to the presence of attractive dipolar interactions in PCL along the c-axis. PCL synthesized through ring-opening polymerization has the dipoles from C(=O)-O groups arranged in a head-to-tail fashion along the chain, resulting in net attractive electrostatic interactions of C(=O)-O groups in neighboring units. These interactions may serve to compress the C-C backbone along c-axis to a greater extent in PCL upon deuteration than in PE, which does not have any dipole groups. The presence of such interactions is also consistent with the shorter length of the aliphatic segment of PCL compared to the equivalent segment of protiated PE (see SI for details). On the other hand, the contraction of lattice parameters in the a, b directions are smaller due to (i) the fact that the dipoles of the carbonyl group C=O within each PCL chain are canceled because of symmetry and (ii) the presence of interchain hydrogen bonding. We will further discuss the dipoles of the ester group and crystal packing in the theoretical section.

Crystallization and Melting Behaviors. Regarding the changes in physical properties as a result of deuteration, we examined the crystallization and melting behaviors. Partially and fully deuterated PCLs exhibit lower melting temperatures than the protiated counterpart when measured by calorimetry.

As the polymers are crystallized at a constant rate of 2.5 $^{\circ}$ C/min and heated at the same rate, melting of the D4-PCL and D10-PCL occurs at lower temperatures than that of the H-PCL (Figure 4a). The $T_{\rm m}$ for D4-PCL and D10-PCL

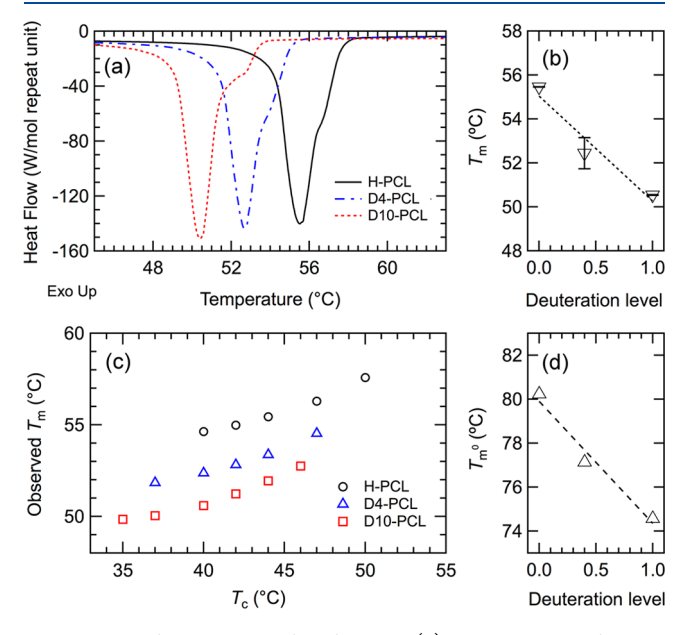


Figure 4. Calorimetry results showing (a) representative heating curves at 2.5 °C/min of PCLs crystallized at the same rate prior to heating, (b) average $T_{\rm m}$ determined from the ramp experiments, (c) $T_{\rm m}$ measured at 10 °C/min after isothermal crystallization at a desired $T_{\rm c}$, and (d) equilibrium melting temperatures $T_{\rm m}^{~0}$ estimated from fitting the results in (c) to a modified Hoffman–Weeks equation. 46 Linear fits to the data points are shown in (b) and (d).

determined from the temperature where the peak maximum occurs appears 3.0 and 4.9 $^{\circ}$ C lower than those for H-PCL, respectively. The plot of $T_{\rm m}$ as a function of deuteration level reveals a nearly linear relationship (Figure 4b). Considering that the melting point of linear PCL increases with increasing DP, ⁴⁶ the small deviation of D4-PCL from the linear trend is not likely from its slightly larger DP (Table 1).

We believe that small differences in the lamellar thickness of the three PCLs are not responsible for the trend in the kinetic melting temperatures. It is well-known that the kinetic melting point of a polymer is proportional to the lamellar thickness as shown in the Gibbs—Thomson equation. The lamellar thickness of the PCLs is analyzed using the samples that are crystallized at the same cooling rate and used for HRPD measurements. The SAXS correlation function (Figure S6) and the extracted structure parameters (Table S1) show that their crystal thickness (L_c) is similar without a clear trend that explains the trend in melting points. Their crystal thickness

Table 3. Melting Temperature $(T_{\rm m})$, Crystallization Temperatures $(T_{\rm c})$, and Enthalpy of Crystallization $(\Delta H_{\rm c})$ from Calorimetry Measurements⁴

polymers	$T_{\rm m} (^{\circ}C)^{b}$	$T_{\rm m}^{\ 0} \ (^{\circ}{\rm C})^{c}$	$T_{c} (^{\circ}C)^{b}$	$\Delta H_{\rm c}^{d}$ (kJ/mol repeat unit)
H-PCL	55.46 ± 0.01	80.23	38.58 ± 0.18	9.83 ± 0.05
D4-PCL	$52.44 \pm 0.85 (-3.02)$	77.13 (-3.10)	$32.70 \pm 0.31 (-5.88)$	9.67 ± 0.09
D10-PCL	$50.54 \pm 0.02 (-4.92)$	74.57 (-5.66)	$33.58 \pm 0.27 (-5.00)$	9.68 ± 0.04

"Average and standard deviation from three separate measurements with temperature ramping at 2.5 °C/min are reported except for $T_{\rm m}^{0}$. $^bT_{\rm m}$ and $T_{\rm c}$ are determined from the temperatures at which the peak maximum occurs. Difference between deuterated and protiated PCL is reported in parentheses. Equilibrium melting temperatures estimated following a previous study. Determined from the area under the crystallization peak. $\Delta H_{\rm c}$ is compared here instead of enthalpy of melting ($\Delta H_{\rm m}$) to avoid overestimation due to melt-recrystallization. $\Delta H_{\rm c}$ is calculated in a molar unit (kJ/molar caprolactone repeat unit) to account for mere mass increase upon deuteration.

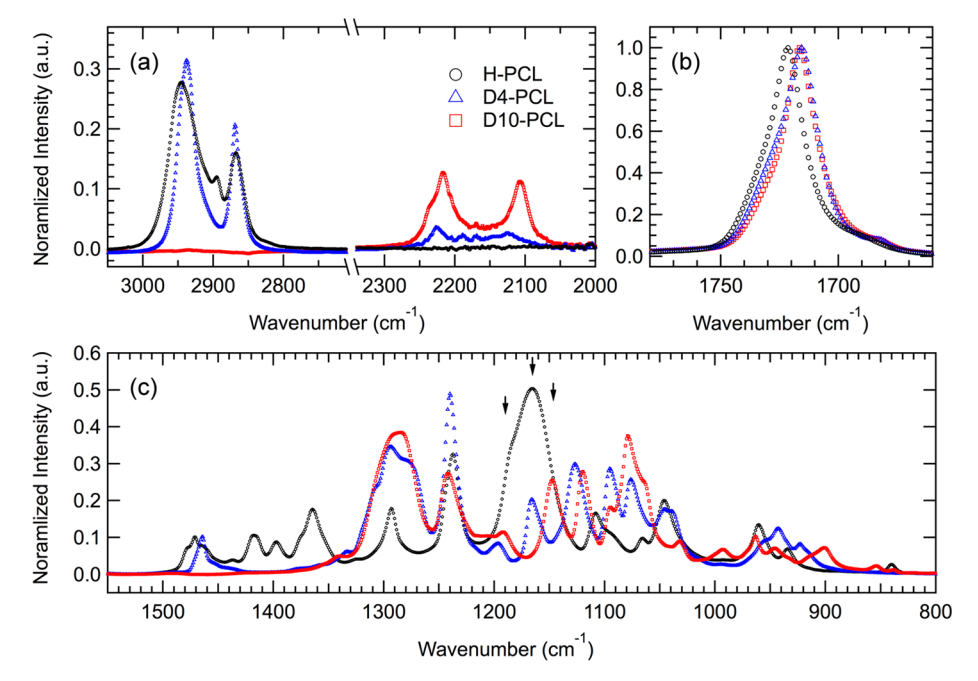


Figure 5. FTIR spectra of H-PCL, D4-PCL, and D10-PCL samples that were crystallized from melt at the same rate. All intensities are normalized to the height of the C=O stretching peaks at 1717–1722 cm⁻¹. Spectral regions are shown for (a) C-H and C-D stretching vibrations, (b) C=O stretching vibrations, and (c) stretching vibrations involving heavier atoms as well as bending vibrations of C-H and C-D. Bands that are related to vibration of ester groups are marked with arrows in (c).

appears to be rather related to their DPs such that the shortest polymer, D10-PCL, has the thickest layer.

Equilibrium melting temperatures $(T_{\rm m}^{~0})$, estimated following the previous report of PCL, ⁴⁶ are also lower for deuterated PCLs. Polymers are isothermally crystallized to approximately 10% of the final crystallinity, and the observed melting temperatures measured at 10 °C/min heating rate are fitted to a modified Hoffman–Weeks equation to extract $T_{\rm m}^{~0}$. Observed melting temperatures of D4-PCL and D10-PCL are consistently lower than that of H-PCL at all crystallization temperatures (Figure 4c). The overall linear trend of the estimated $T_{\rm m}^{~0}$ as a function of deuteration level is very similar to that of the kinetic melting points (Figure 4d). These calorimetry results are summarized in Table 3.

Melting point depression of deuterated polymers has been primarily attributed to their weaker intermolecular interactions in the literature. Bates et al. have proposed an equation that predicts melting point depression of nonpolar polymers by assuming that (i) $T_{\rm m}$ is proportional to the strength of attractive interaction energy and (ii) attractive interactions of nonpolar polymers can be described by London dispersion forces that depend on polarizability of molecules and distance between them (which is inversely proportional to molar

volume). This reasoning has been successfully used in predicting $T_{\rm m}$ depression of nonpolar polymers such as PE, iPS, and iPP. Applying the equation to D10-PCL with the measured molar volume ratio (1.0061), the estimated $T_{\rm m}^{~0}$ of H-PCL (353.4 K), and the polarizability ratio borrowed from the PE system (1.011), the melting point depression is predicted to be approximately 3.4 °C, smaller than the observed 4.9 °C. We believe that this discrepancy could result from the fact that interactions between PCLs cannot be fully described by the dispersion forces alone. In fact, analysis of crystal packing suggests that some of the H/D atoms in PCL are involved in a weak hydrogen bonding with the carbonyl group, which slightly polarizes the C–H bond and introduces an electrostatic contribution. Interactions of PCL resulting from the presence of carbonyl groups will be further discussed in the theoretical section later.

While only a few studies have been reported concerning the effect of partial deuteration on $T_{\rm m}$ depression compared to full deuteration, the generally linear trend in this work is consistent with a previous report on partially deuterated PEs. PEs with deuteration levels 0.19 and 0.59 display $1-2~^{\circ}{\rm C}$ lower melting points compared to nondeuterated PE, suggesting a linear relationship between melting point depression and deuteration

level. The consistent results from the two separate studies are interesting because partially deuterated PEs have statistical distribution of D along the chain (obtained from H/D exchange reaction after polymerization), while the D atoms in D4-PCL are precisely positioned in this study. A partially deuterated sPP with statistical H/D distribution is recently reported to display an unusually large $T_{\rm m}$ depression of 12.5 °C at deuteration level 0.26. Although no information is available about the $T_{\rm m}$ of fully deuterated sPP, isotactic polypropylene (iPP) displays 3–5 °C $T_{\rm m}$ depression upon full deuteration. Nevertheless, the melting point depression in this work results from deuteration itself and the resultant weaker C–D bond polarizability, not from the inhomogeneous distribution of H/D.

The crystallization kinetics for D4-PCL are surprisingly slower than both H-PCL and D10-PCL and warrant further investigation. The large T_c depression of D4-PCL significantly deviating from the linear trend (Table 3) and its asymmetric peak shape in cooling scans (data not shown) compared to the isotopically pure PCLs (H-PCL and D10-PCL) are consistently observed in multiple measurements. The large variation in crystallization kinetics is also reflected in the relatively large standard deviation in T_m measurements compared to the other two PCLs, such that cooling curves with lower Tc's are followed by heating curves with relatively higher $T_{\rm m}$'s. Connection between the seemingly slower crystallization kinetics of D4-PCL and its isotopic inhomogeneity is not very conclusive due to the slightly larger DP of D4-PCL in this work. Crist et al. reported similar results, where 59% deuterated PE displayed a 3.8 °C lower $T_{\rm c}$ while its $T_{\rm m}$ is lower by 2 °C. ²¹ Whether the slow crystallization kinetics of partially deuterated polymers are universal and how isotopic inhomogeneity and the distribution of H/D affect crystallization kinetics will require careful investigation.

The enthalpy change of phase transition shows only small differences (Table 3). Theoretically, weaker intermolecular interactions of deuterated PCLs should manifest smaller enthalpy changes upon crystallization; however, the differences in their enthalpy change are within standard deviations in our multiple experiments. The volume crystallinity analysis from SAXS (Table S1) and HRPD curves (Figure 2) also suggest similar crystallinity of the three PCLs. We conclude that deuteration does not have as significant an impact on the crystallinity of PCL as compared to a previously investigated conjugated polymer.¹⁴

Fourier-Transform Infrared Spectroscopy. Next, we studied the changes of vibrational properties caused by deuteration. FTIR spectra of semicrystalline PCLs measured at room temperature are shown in Figure 5. The intensities are normalized to the height of the C=O stretching peak in the crystalline phase, assuming that the dipole moment change associated with this stretching is minimally affected by deuteration and that the crystallinities of all three samples are similar. It is immediately clear that frequency and intensity of the C-H and C-D stretching vibrations are qualitatively consistent with their deuteration level (Figure 5a). H-PCL displays two main peaks centered at 2945 and 2868 cm⁻¹ that can be assigned to asymmetric and symmetric stretching of methylene groups in PCL, respectively. 54 The small peak at 2895 cm⁻¹ is either not assigned in the literature⁵⁴ or assigned to a symmetric CH₂ stretching in the crystalline phase; 5. however, the lack of this signal in D4-PCL suggests that it is related to stretching of the methylene group(s) adjacent to the

ester group. Two sharp peaks of D4-PCL in the C–H stretching region match well with those of H-PCL and are likely from asymmetric and symmetric stretching of the nondeuterated methylene groups. The decreased overall area for the C–H stretching peaks as well as the emergence of new peaks in the 2000–2300 cm⁻¹ region of D4-PCL, which is shifted approximately by a factor of $\sqrt{m_{\rm H}/m_{\rm D}}$ (where $m_{\rm H}$ and $m_{\rm D}$ denote the atomic masses of H and D, respectively), is consistent with the partial deuteration. Stronger peaks from D10-PCL in this region as well as its lack of C–H stretching bands confirm its full deuteration. Overall, the total stretching peak area for H-PCL is larger than that for D10-PCL, which is consistent with the lower polarizability of the C–D bond. 14

Carbonyl stretching frequency, which is known to be sensitive to its environment, shows a small red shift upon deuteration of the adjacent C atoms (Figure 5b). The C=O stretching peak appears at 1722 cm⁻¹ for H-PCL, which is reasonably consistent with the reported value 1724 cm⁻¹ for a crystalline PCL.55 The peaks for D4-PCL and D10-PCL are shifted toward lower wavenumber at 1717 cm⁻¹. The fact that stretching frequencies for D4-PCL and D10-PCL are identical within the experimental resolution suggests the shift primarily arises from deuteration of the two C atoms immediately adjacent to the carbonyl group. The origin of the red shift is explained in the simulation section in detail. Additionally, contribution of C=O in the amorphous phase appears as a shoulder centered around 1736 cm⁻¹ for H-PCL as reported in literature. 55,56 The C=O stretching in the amorphous phase of D4-PCL and D10-PCL is red-shifted to the same degree as in the crystalline phase according to a separate FTIR measurement of melt PCL samples (Figure S7).

Vibrational modes involving the ester group are also significantly affected by deuteration, although the high complexity in the fingerprint region hinders complete assignment (Figure 5c). Peaks in the 1100-1300 cm⁻¹ region are associated with C-C-H bending, O-C-H bending, C-C stretching, and C-O stretching. 55 The intense band centered around 1166 cm⁻¹ for H-PCL can be deconvoluted into three peaks at 1190, 1170, and 1157 cm⁻¹ assigned to C(=O)-O stretching, symmetric C(=O)-O-C stretching, and combination of C-O and C-C stretching in the amorphous state, respectively.⁵⁴ FTIR spectra of D4-PCL and D10-PCL in this region do not show clear frequency scaling with the isotope mass, i.e. $\sqrt{m_{\rm H}/m_{\rm D}}$, since most peaks in this spectral region are associated with the skeletal vibrations of heavy atoms. Full spectra between 4000 and 400 cm⁻¹ are shown in Figure 7b in comparison with predicted FTIR spectra.

Theoretical Analysis Based on the Electronic Structure Calculations. Using the DFT calculations, we attempted to obtain further understanding of the effect of deuteration on the interaction and dynamics of PCL. The structural model for PCL shown in Figure 6 was constructed based on an experimental structure obtained from XRD. According to the XRD results by Chatani et al.,³⁶ the PCL chains are slightly nonplanar, as seen from the view along the PCL chains in Figure 6a. At the same time, Bittiger and Marchessault reported that the polymers are planar.⁴⁷ However, the nonplanarity was confirmed by Hu and Dorset using the electron diffraction two decades later.⁴⁸ In order to understand deuteration effects on the vibrational modes of PCLs, we have fixed the lattice parameters according to the results from Chatani et al.³⁶

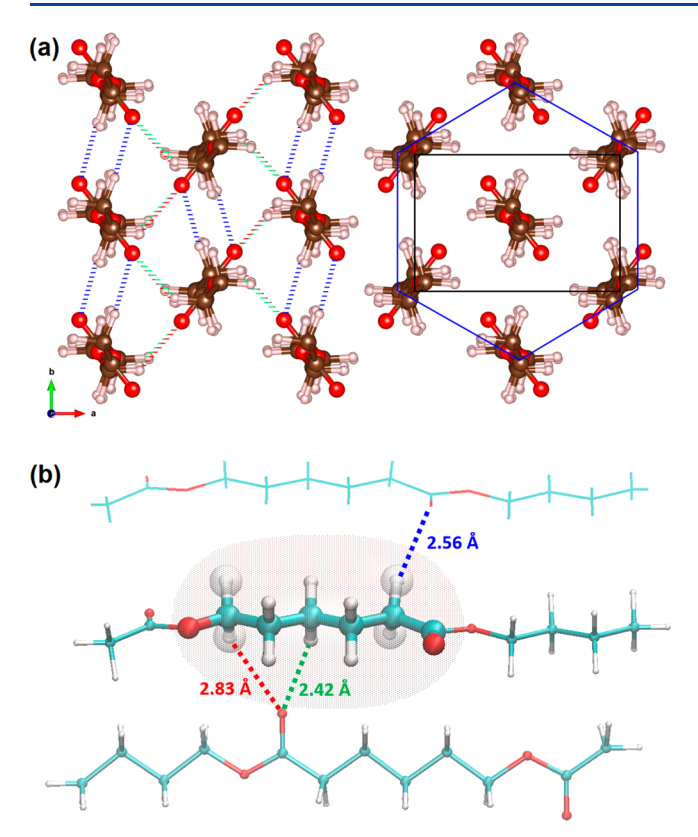


Figure 6. (a) Top view along the *c*-axis (or the chains) of the PCL crystal structure based on the XRD data from the literature. The black rectangular box indicates the primitive cell that consists of 2 chains. The blue hexagonal box indicates the hexagonal close packing motif used to construct the 7-chain cluster model. (b) Side view of three PCL chains taken from the cluster model. The shaded area shows a single caprolactone unit in the PCL crystal with respect to neighboring PCL chains. The positions of deuterium in D4-PCL are marked as spheres around the atoms. Three H atoms in each caprolactone repeat unit form weak H-bonds with the carbonyl groups on neighboring PCL chains. In both panels, weak H-bonds with C=O···H distances ranging from 2.42, 2.56, to 2.83 Å are represented by green, blue, and red dashed lines, respectively.

The crystal structure of PCL belongs to the $P2_12_12_1$ space group. The primitive cell contains two chains that tilt differently (black rectangular box in Figure 6a). A careful examination indicates that the crystal structure consists of alternating layers of PCL chains along the a-axis. Within each layer, the chains are parallel to each other and all tilt in one direction, but those in neighboring layers all tilt differently. This gives rise to a herringbone-like packing motif. Alternatively, neighboring PCL chains form a hexagonal-like close packing (blue hexagonal box in Figure 6a). All ester groups within each layer point in the same direction along the chain (or the c-axis), but they flip directions in neighboring layers, giving ordered antiferroelectric arrangements of dipoles on ester groups. As mentioned in the earlier discussion on the lattice parameter changes, each carbonyl group (C=O) also creates a local dipole that is perpendicular to the chain (or the c-axis), but the overall dipole of each chain in the perpendicular direction is canceled due to the 2₁ screw axis.

Further analysis of the crystal structure reveals that each O atom in the carbonyl group (C=O) forms three close contacts with the H atoms on neighboring chains (shown in Figure 6 by color-coded dashed line with distances of 2.42, 2.56, and 2.83

Å). Due to the electronegativity of C being greater than that of H but smaller than those of F, O, and N in typical H-bonds, this proximity may lead to weak H-bond-like interactions.⁵ We emphasize that such weak interactions may form a dense network to hold the PCL chains together in addition to the dispersion forces. As shown in Figure 6a, the intermediate 2.56 Å contact is between PCL chains within the same layer, while the shortest 2.42 Å and the longest 2.83 Å contacts exist between the chains from the neighboring layers. Another way to look at this is from the perspective of the aliphatic segment C_5H_{10} (Figure 6b). Three out of the ten H atoms in C_5H_{10} are involved in the close contacts, two of which are immediately adjacent to the ester group. Therefore, these two H-bond-like interactions will be affected by deuteration in both D4-PCL and D10-PCL. The third one is associated with the H-atom located in the center of the aliphatic segment and therefore is affected only by deuteration in D10-PCL.

To rationalize the change of vibrational property caused by selective deuteration, we calculated the IR spectrum of a single caprolactone unit located in the central chain of a 7-chain cluster model while treating all remaining atoms frozen. First, the 18 atoms in the shaded region of Figure 6b were optimized. Then, given the size of the cluster model of 266 atoms, the Hessian matrix was calculated numerically from analytical gradients using the finite difference method. The IR spectra were obtained from this partial Hessian matrix corresponding to the selected single caprolactone unit. The resulting theoretical IR spectra for H-PCL and D10-PCL (no scaling is applied) are shown on Figure 7a and compared to the experimental FTIR data in Figure 5. Although the calculations did not include the phonon modes or dynamic

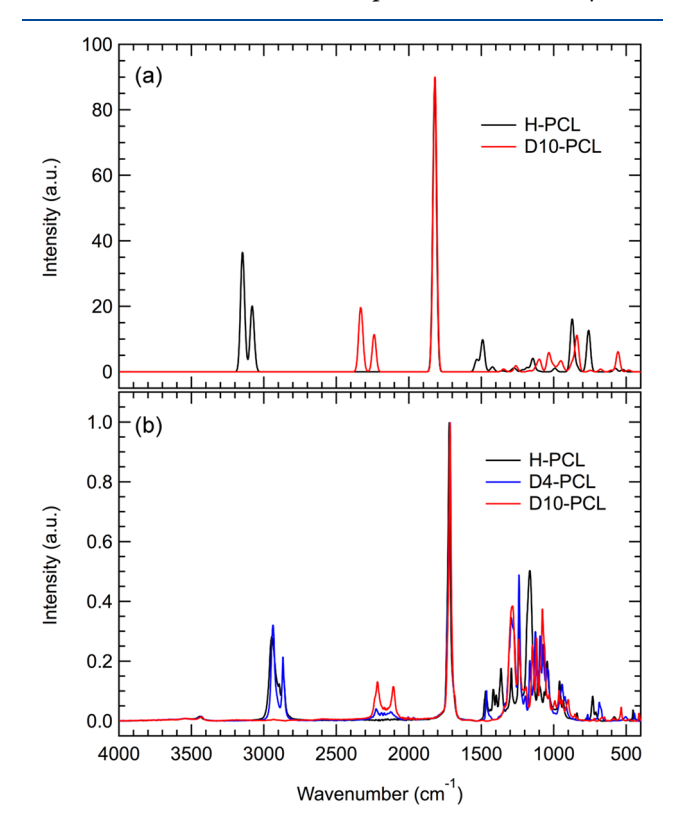


Figure 7. Theoretical (a) versus experimental (b) IR spectra for H-PCL and D10-PCL. Only a single caprolactone repeat unit was considered in the current simulations.

I

interactions with neighboring chains, the agreement between the theoretical and experimental IR spectra is excellent for frequencies above 1500 $\rm cm^{-1}$. The usual blue shift is partly attributed to an incomplete basis set used in the calculations. Our focuses are on the stretching peaks for the methylene CH₂ and carbonyl C=O groups, especially, on their changes upon isotope substitution.

The peaks at ~ 3100 cm⁻¹ (slightly higher than the experimental values at ~2900 cm⁻¹) correspond to the asymmetric and symmetric stretching of CH₂ in H-PCL. Analogous modes of CD₂ in D10-PCL and D4-PCL appear at lower frequencies near 2300 cm⁻¹ in simulations and near 2200 cm⁻¹ in experiments. This shift corresponds to the usual frequency scaling, $\sqrt{m_{\rm D}/m_{\rm H}} = \sqrt{2}$, due to H/D substitution. More precisely, the simulated shift corresponds to a scaling factor of 1.35–1.37 rather than $\sqrt{2}$. This is explained if one uses reduced masses of C–H ($\mu_{\rm CH}$ = 12/13) and C–D ($\mu_{\rm CD}$ = 12/7) bonds instead of the H/D masses, i.e., $\sqrt{\mu_{\rm CD}}/\mu_{\rm CH} = \sqrt{13/7}$. As seen in Figure 7, the stretching mode of the carbonyl group C=O appears at \sim 1800 cm⁻¹ and it red shifts by 3.5 cm⁻¹ upon deuteration. This is consistent with the experimental red shift of 5 cm⁻¹ from 1722 cm⁻¹ for H-PCL to 1717 cm⁻¹ for D4-PCL and D10-PCL (Figures 5b and 7b). Please note that the carbonyl stretching frequencies for D4-PCL and D10-PCL are almost identical. Thus, this red shift can be attributed mainly to the change in the reduced mass of the C=O oscillator upon deuteration at the positions adjacent to the ester group. The remaining six H atoms are further away (in terms of the bond distance) from the carbonyl group and show no significant influence on the C=O vibration.

In the calculations discussed so far, the vibration of the C= O group in a given caprolactone repeat unit is decoupled from the environment besides the static crystal field coming from the frozen PCL fragment surrounding the active caprolactone unit. (The Hessian matrix was calculated only over the coordinates of active caprolactone unit and not on the neighboring units.) However, as illustrated in Figure 6b, the O-atom of the carbonyl group interacts with 3 H-atoms through weak H-bond-like interactions. To evaluate the effect of the interchain interaction on the C=O mode of the IR spectrum, we have extended the partial Hessian analysis to 28 atoms of the central chain of the 7-chain cluster model (see Figure S8 for additional details). In this model the C=O stretching frequency red shifts by 3.53 cm⁻¹ upon deuteration. Inclusion of three additional H-atoms, nearest to the central C=O group and weakly bonding to its oxygen, gives a small additional red shift of 0.12 cm⁻¹, leading to a slightly larger red shift of 3.65 cm⁻¹. Inclusion of three D-atoms in place of Hatoms has negligible effect on this mode's frequency. The mode composition is consistent with this observation: contribution from 3 "close contact" hydrogen atoms to this mode is 0.3% while it is only 0.1% for the deuterium atoms. This additional red shift of 0.12 cm⁻¹ is small, but is likely underestimated within the normal-mode analysis, given high anharmonicity of weak interactions, which is typical of Hbonds. Thus, we attribute the experimentally observed 5 cm⁻¹ red shift for the deuterated species to the combined effects of the reduced mass change (intrachain effect) and of the dynamical coupling of the C=O group with the vibrations of C-H and C-D bonds through weak H-bond-like interactions (interchain effect).

Finally, we would like to comment on the fingerprint region. The experimental FTIR spectra show additional features below 1500 cm⁻¹, which appear to be much denser than the theoretical results. This discrepancy can be attributed to the intra- and interchain couplings between different caprolactone repeat units in the PCL crystal not fully captured in the normal modes analysis. Based on our calculations, the vibrations in the fingerprint region consist of bending modes of the CH₂ group, i.e., scissoring, wagging, twisting, and rocking, in the order of decreasing frequencies, and the vibrations of the polymer chain's backbone. For instance, the main features include CH₂'s scissoring at 1491 cm⁻¹ and rocking at 760 cm⁻¹ for H-PCL, which are red-shifted to 1104 and 558 cm⁻¹ for D10-PCL, both by a factor of $\sqrt{13/7}$. Consequently, the backbone vibrations start to emerge on the higher frequency side of the fingerprint region upon deuteration. One relatively strong feature of the backbone vibrations is the ester group's stretching at 878 cm⁻¹, which is red shifted to 840 cm⁻¹ upon full deuteration. Detailed vibration analysis is in progress. The geometry and setup of the presented calculations are given in the Supporting Information.

4. CONCLUSIONS AND OUTLOOK

Selectively deuterated PCLs are designed and synthesized, and the effects of isotopic substitution on the crystal structures and the fundamental physical properties of resultant PCLs are also investigated. Analysis of their crystal structures using highresolution synchrotron X-ray diffraction shows that their crystal lattice parameters linearly decrease with increasing level of deuteration. Unexpectedly, PCLs show large c-axis reduction of their orthorhombic lattices upon deuteration compared to previously reported PE systems. The unique behavior is ascribed to the presence of net attractive dipolar interactions along the c-axis due to the arrangement of ester groups along PCL chains. Melting point depressions that are also linearly proportional to the deuteration level support the previous explanation about weaker intermolecular interactions of deuterated polymers. Red shifts in the carbonyl stretching vibration frequency are observed for deuterated PCLs. This frequency shift is confirmed by simulations to be a combined effect of the larger reduced mass of the vibrational units and, possibly, by the weak hydrogen-bond-like interchain interactions. Large red shifts of the vibrational frequencies for the stretching and bending modes of C-D versus C-H bonds are dictated by their relative reduced masses.

Deuteration effects on crystal lattice parameters and melting temperatures of PCL quantified in this study may be small, with an approximately 1.6% change for the estimated $T_{\rm m}^{0}$ of D10-PCL -PCL at most. Such subtle effects are not expected to play a significant role in most experimental designs employing deuterated polymers. However, the unexpected crystallization kinetics of isotopically inhomogeneous PCLs, i.e. partially deuterated PCLs, certainly merits more thorough studies using various methods (including small angle neutron scattering). It may offer a new avenue to design polymers with desired structures and properties.

ASSOCIATED CONTENT

S Supporting Information

The Supporting Information is available free of charge on the ACS Publications website at DOI: 10.1021/acs.macromol.8b01851.

Additional synthetic and experimental details and characterization data (PDF)

AUTHOR INFORMATION

Corresponding Authors

*E-mail: changd@ornl.gov (D.C.). *E-mail: hongkq@ornl.gov (K.H.).

ORCID ©

Jacek Jakowski: 0000-0003-4906-3574 Jingsong Huang: 0000-0001-8993-2506 Byeongdu Lee: 0000-0003-2514-8805 Sophya Garashchuk: 0000-0003-2452-7379 Bobby G. Sumpter: 0000-0001-6341-0355 Kunlun Hong: 0000-0002-2852-5111

Notes

The authors declare no competing financial interest.

ACKNOWLEDGMENTS

This work was performed at the Center for Materials Sciences which is a U.S. Department of Energy (DOE) Office of Science User Facility and LL was partially supported by the National Science Foundation under Grant Nos. CHE-1056188, OIA-1655740 and by SC EPSCoR/IDeA 18-GE02 (S.G.). This research used resources of the Advanced Photon Source, a U.S. Department of Energy Office of Science User Facility operated for the DOE Office of Science by Argonne National Laboratory under Contract No. DE-AC02-06CH11357. We thank Professor Megan L. Robertson (University of Houston, TX) and Ms. Avantika Singh for information regarding caprolactone synthesis using Bi(OTf)₃-catalyzed Baeyer-Villager reactions. Computations used resources of the National Energy Research Scientific Computing Center supported by the DOE Office of Science under Contract No. DE-AC02-05CH11231 and resources at the University of South Carolina funded under Grant No. CHE-1048629.

REFERENCES

- (1) Chen, S. H. Small Angle Neutron Scattering Studies of the Structure and Interaction in Micellar and Microemulsion Systems. *Annu. Rev. Phys. Chem.* **1986**, 37 (1), 351–399.
- (2) Schurtenberger, P. Contrast and Contrast Variation in Neutron, X-Ray, and Light Scattering. In *Neutrons, X-rays and Light: Scattering Methods Applied to Soft Condensed Matter*; Lindner, P., Zemb, T., Eds.; North-Holland: Amsterdam, The Netherlands, 2002.
- (3) Wignall, G. D.; Melnichenko, Y. B. Recent Applications of Small-Angle Neutron Scattering in Strongly Interacting Soft Condensed Matter. *Rep. Prog. Phys.* **2005**, *68* (8), 1761–1810.
- (4) Schmidt-Rohr, K.; Hu, W.; Zumbulyadis, N. Elucidation of the Chain Conformation in a Glassy Polyester, PET, by Two-Dimensional NMR. *Science (Washington, DC, U. S.)* **1998**, 280 (5364), 714–717.
- (5) Schmidt-Rohr, K.; Spiess, H. W. Multidimensional Solid-State NMR and Polymers; Elsevier Science: 2012.
- (6) Hong, Y. L.; Chen, W.; Yuan, S.; Kang, J.; Miyoshi, T. Chain Trajectory of Semicrystalline Polymers As Revealed by Solid-State NMR Spectroscopy. ACS Macro Lett. 2016, 5 (3), 355–358.
- (7) Mitra, I.; Li, X.; Pesek, S. L.; Makarenko, B.; Lokitz, B. S.; Uhrig, D.; Ankner, J. F.; Verduzco, R.; Stein, G. E. Thin Film Phase Behavior of Bottlebrush/Linear Polymer Blends. *Macromolecules* **2014**, 47 (15), 5269–5276.
- (8) Olsen, B. D.; Li, X.; Wang, J.; Segalman, R. A. Thin Film Structure of Symmetric Rod-Coil Block Copolymers. *Macromolecules* **2007**, *40* (9), 3287–3295.

- (9) Cannon, C. G. The Infra-Red Spectra and Molecular Configurations of Polyamides. *Spectrochim. Acta* **1960**, *16* (26), 302–319.
- (10) Lee, Y. J.; Snyder, C. R.; Forster, A. M.; Cicerone, M. T.; Wu, W. Imaging the Molecular Structure of Polyethylene Blends with Broadband Coherent Raman Microscopy. *ACS Macro Lett.* **2012**, *1* (11), 1347–1351.
- (11) White, R. P.; Lipson, J. E. G.; Higgins, J. S. Effect of Deuterium Substitution on the Physical Properties of Polymer Melts and Blends. *Macromolecules* **2010**, *43* (9), 4287–4293.
- (12) Shao, M.; Keum, J.; Chen, J.; He, Y.; Chen, W.; Browning, J. F.; Jakowski, J.; Sumpter, B. G.; Ivanov, I. N.; Ma, Y.-Z.; et al. The Isotopic Effects of Deuteration on Optoelectronic Properties of Conducting Polymers. *Nat. Commun.* **2014**, *5*, 3180.
- (13) Wang, L.; Jakowski, J.; Garashchuk, S.; Sumpter, B. G. Understanding How Isotopes Affect Charge Transfer in P3HT/PCBM: A Quantum Trajectory-Electronic Structure Study with Nonlinear Quantum Corrections. *J. Chem. Theory Comput.* **2016**, *12* (9), 4487–4500.
- (14) Jakowski, J.; Huang, J.; Garashchuk, S.; Luo, Y.; Hong, K.; Keum, J.; Sumpter, B. G. Deuteration as a Means to Tune Crystallinity of Conducting Polymers. *J. Phys. Chem. Lett.* **2017**, 8, 4333–4340.
- (15) Garashchuk, S.; Huang, J.; Sumpter, B. G.; Jakowski, J. Theoretical Assessment of the Nuclear Quantum Effects on Polymer Crystallinity via Perturbation Theory and Dynamics. *Int. J. Quantum Chem.* Early View: 2018, 118, e25712https://doi.org/10.1002/qua. 25712.
- (16) Bates, F. S.; Keith, H. D.; Mcwhan, D. B. Isotope Effect on the Melting Temperature of Nonpolar Polymers. *Macromolecules* **1987**, *20* (12), 3065–3070.
- (17) Stehling, F. C.; Ergos, E.; Mandelkern, L. Phase Separation in n-Hexatriacontane-n-Hexatriacontane- d_{74} and Polyethylene—Poly-(Ethylene- d_4) Systems. *Macromolecules* **1971**, 4 (6), 672–677.
- (18) English, A. D.; Smith, P. Polyethylene/Deutero-Polyethylene Phase Behaviour. *Polymer* 1985, 26 (10), 1523–1526.
- (19) Guenet, J. M.; Picot, C.; Benoit, H. Chain Conformation of Isotactic Polystyrene in the Bulk Amorphous State as Revealed by Small-Angle Neutron Scattering. *Macromolecules* **1979**, *12* (1), 86–90.
- (20) Mezghani, K.; Phillips, P. J. Equilibrium Melting Point of Deuterated Polypropylene. *Macromolecules* **1994**, 27 (21), 6145–6146.
- (21) Crist, B.; Nicholson, J. C. Small-Angle Neutron-Scattering Studies of Partially Labelled Crystalline Polyethylene. *Polymer* **1994**, 35 (9), 1846–1854.
- (22) Habersberger, B. M.; Baugh, D. W. Solvent and Polymer Stereochemistry Play Key Roles in Deuterium Exchange and Partial Racemization of Polypropylenes. *Macromolecules* **2018**, *51* (4), 1290–1295.
- (23) Bates, F. S.; Dierker, S. B.; Wignall, G. D. Phase Behavior of Amorphous Binary Mixtures of Perdeuterated and Normal 1,4-Polybutadienes. *Macromolecules* **1986**, *19* (7), 1938–1945.
- (24) Bates, F. S.; Fetters, L. J.; Wignall, G. D. Thermodynamics of Isotopic Polymer Mixtures: Poly(Vinylethylene) and Poly-(Ethylethylene). *Macromolecules* 1988, 21 (4), 1086–1094.
- (25) Bartell, L. S.; Roskos, R. R. Isotope Effects on Molar Volume and Surface Tension: Simple Theoretical Model and Experimental Data for Hydrocarbons. *J. Chem. Phys.* **1966**, *44* (2), 457–463.
- (26) Lacks, D. J. Origins of Molar Volume Isotope Effects in Hydrocarbon Systems. *J. Chem. Phys.* **1995**, *103* (12), 5085–5090.
- (27) Labet, M.; Thielemans, W. Synthesis of Polycaprolactone: A Review. *Chem. Soc. Rev.* **2009**, 38 (12), 3484.
- (28) Gross, R. A.; Kalra, B. Biodegradable Polymers for the Environment. *Science* **2002**, 297 (5582), 803–807.
- (29) Woodruff, M. A.; Hutmacher, D. W. The Return of a Forgotten Polymer Polycaprolactone in the 21st Century. *Prog. Polym. Sci.* **2010**, 35 (10), 1217–1256.

(30) Ulery, B. D.; Nair, L. S.; Laurencin, C. T. Biomedical Applications of Biodegradable Polymers. J. Polym. Sci., Part B: Polym. Phys. 2011, 49 (12), 832-864.

- (31) Phillips, P. J.; Rensch, G. J.; Taylor, K. D. Crystallization Studies of Poly(ε -Caprolactone).I. Morphology and Kinetics. *J. Polym.* Sci., Part B: Polym. Phys. 1987, 25 (8), 1725-1740.
- (32) Phillips, P. J.; Rensch, G. J. Crystallization Studies of Poly(ε caprolactone). II. Lamellar Thickening and Melting. J. Polym. Sci., Part B: Polym. Phys. 1989, 27 (1), 155-173.
- (33) Jenkins, M. J.; Harrison, K. L. The Effect of Molecular Weight on the Crystallization Kinetics of Polycaprolactone. Polym. Adv. Technol. 2006, 17 (April), 474-487.
- (34) Wurm, A.; Zhuravlev, E.; Eckstein, K.; Jehnichen, D.; Pospiech, D.; Androsch, R.; Wunderlich, B.; Schick, C. Crystallization and Homogeneous Nucleation Kinetics of Poly(ε -Caprolactone) (PCL) with Different Molar Masses. Macromolecules 2012, 45 (9), 3816-
- (35) Möller, M.; Kånge, R.; Hedrick, J. L. Sn(OTf)2 and Sc(OTf)3: Efficient and Versatile Catalysts for the Controlled Polymerization of Lactones. J. Polym. Sci., Part A: Polym. Chem. 2000, 38 (11), 2067-
- (36) Chatani, Y.; Okita, Y.; Tadokoro, H.; Yamashita, Y. Structural Studies of Polyesters. III. Crystal Structure of Poly-\varepsilon-Caprolactone. Polym. J. 1970, 1, 555-562.
- (37) Perdew, J. P.; Burke, K.; Ernzerhof, M. Generalized Gradient Approximation Made Simple. Phys. Rev. Lett. 1996, 77 (18), 3865.
- (38) Hafner, J. Ab-initio Simulations of Materials Using VASP: Density-functional Theory and Beyond. J. Comput. Chem. 2008, 29 (13), 2044-2078.
- (39) Blöchl, P. E. Projector Augmented-Wave Method. Phys. Rev. B: Condens. Matter Mater. Phys. 1994, 50 (24), 17953-17979.
- (40) Kresse, G.; Joubert, D. From Ultrasoft Pseudopotentials to the Projector Augmented-Wave Method. Phys. Rev. B: Condens. Matter Mater. Phys. 1999, 59 (3), 1758-1775.
- (41) Shao, Y.; Gan, Z.; Epifanovsky, E.; Gilbert, A. T. B.; Wormit, M.; Kussmann, J.; Lange, A. W.; Behn, A.; Deng, J.; Feng, X.; et al. Advances in Molecular Quantum Chemistry Contained in the Q-Chem 4 Program Package. Mol. Phys. 2015, 113 (2), 184-215.
- (42) Rohrdanz, M. A.; Martins, K. M.; Herbert, J. M. A Long-Range-Corrected Density Functional That Performs Well for Both Ground-State Properties and Time-Dependent Density Functional Theory Excitation Energies, Including Charge-Transfer Excited States. J. Chem. Phys. 2009, 130 (5), 54112.
- (43) Tabet, J. C.; Doan, D.; Longeray, R.; Fraisse, D.; Suon, K. Molecular Isomerization and Fragmentation of Caprolactone upon Electron Impact. Int. J. Mass Spectrom. Ion Phys. 1983, 47 (C), 407-
- (44) Ottewill, R. H.; Rennie, A. R.; Laughlin, R. G.; Bunke, G. M. Micellar Structure in Solutions of an Ultralong Chain Zwitterionic Surfactant. Langmuir 1994, 10 (10), 3493-3499.
- (45) Alam, M. M.; Varala, R.; Adapa, S. R. Bi(OTf)3-Catalyzed Baeyer-Villiger Oxidation of Carbonyl Compounds with m-CPBA. Synth. Commun. 2003, 33 (17), 3035-3040.
- (46) Núñez, E.; Ferrando, C.; Malmström, E.; Claesson, H.; Werner, P. E.; Gedde, U. W. Crystal Structure, Melting Behaviour and Equilibrium Melting Point of Star Polyesters with Crystallisable Poly(ε -Caprolactone) Arms. *Polymer* **2004**, 45 (15), 5251–5263.
- (47) Bittiger, H.; Marchessault, R. H.; Niegisch, W. D. Crystal Structure of Poly-\varepsilon-Caprolactone. Acta Crystallogr., Sect. B: Struct. Crystallogr. Cryst. Chem. 1970, 26, 1923.
- (48) Hu, H.; Dorset, D. L. Crystal Structure of Poly(ϵ -Caprolactone). Macromolecules 1990, 23 (21), 4604-4607.
- (49) Sadler, D. M.; Keller, A. Neutron Scattering Studies on the Molecular Trajectory in Polyethylene Crystallized from Solution and Melt. Macromolecules 1977, 10 (5), 1128-1140.
- (50) Rastogi, S.; Lippits, D. R.; Terry, A. E.; Lemstra, P. J. The Role of the Interphase on the Chain Mobility and Melting of Semi-Crystalline Polymers; A Study on Polyethylenes. In Progress in understanding of polymer crystallization; Springer: 2007; pp 285-327.

(51) Piorkowska, E.; Rutledge, G. C. Handbook of Polymer Crystallization; John Wiley & Sons: 2013.

- (52) Shearer, H. M. M.: Vand, V. The Crystal Structure of the Monoclinic Form of N-Hexatriacontane. Acta Crystallogr. 1956, 9 (4), 379 - 384.
- (53) Kossack, W.; Seidlitz, A.; Thurn-Albrecht, T.; Kremer, F. Molecular Order in Cold Drawn, Strain-Recrystallized Poly(ε-Caprolactone). Macromolecules 2017, 50 (3), 1056-1065.
- (54) Elzein, T.; Nasser-Eddine, M.; Delaite, C.; Bistac, S.; Dumas, P. FTIR Study of Polycaprolactone Chain Organization at Interfaces. J. Colloid Interface Sci. 2004, 273 (2), 381-387.
- (55) Coleman, M. M.; Zarian, J. Fourier-Transform Infrared Studies of Polymer Blends. II. Poly(ε -Caprolactone)-Poly(Vinyl Chloride) System. J. Polym. Sci., Polym. Phys. Ed. 1979, 17 (5), 837-850.
- (56) He, Y.; Inoue, Y. Novel FTIR Method for Determining the Crystallinity of Poly(ε -Caprolactone). Polym. Int. **2000**, 49 (6), 623–
- (57) Sato, H.; Nakamura, M.; Padermshoke, A.; Yamaguchi, H.; Terauchi, H.; Ekgasit, S.; Noda, I.; Ozaki, Y. Thermal Behavior and Molecular Interaction of Poly(3-hydroxybutyrate-co-3-hydroxyhexanoate) Studied by Wide-Angle X-Ray Diffraction. Macromolecules 2004, 37 (10), 3763-3769.